Optical and thermal properties of commercial polymer film, modelling the albedo effect

Received: 3 November 2020 | Revised: 25 January 2021 | Accepted: 26 January 2021

DOI: 10.1002/app.50581

ARTICLE

Applied Polymer SCIENCE WILEY

Optical and thermal properties of commercial polymer film, modeling the albedo effect

Saeed D. Mohan[1] | Fred J. Davis[1] | Amir Badiee[2] | Paul Hadley[3] | Carrie-Anne Twitchen[3] | Simon Pearson[2] | Ken Gargan[4]

[1]Department of Chemistry, University of Reading, Reading, UK

[2]Lincoln Institute for Agri-Food Technology, University of Lincoln, Lincoln, UK

[3]Department of Agriculture, University of Reading, Reading, UK

[4]BPI Agriculture, RPC BPI, Stevenston, UK

Correspondence
Saeed D. Mohan and Fred J. Davis, Department of Chemistry, University of Reading, Whiteknights, Reading, RG6 6AD, UK.
Email: s.mohan2@reading.ac.uk (S. D. M.) and f.j.davis@reading.ac.uk (F. J. D.)

Abstract

Greenhouse cladding materials are an important part of greenhouse design. The cladding material controls the light transmission and distribution over the plants within the greenhouse, thereby exerting a major influence on the overall yield. Greenhouse claddings are typically translucent materials offering more diffusive transmission than reflection; however, the reflective properties of the films offer a potential route to increasing the surface albedo of the local environment. We model thermal properties by modeling the films based on their optical transmissions and reflections. We can use this data to estimate their albedo and determine the amount of short wave radiation that will be transmitted/reflected/blocked by the materials and how it can influence the local environment.

KEYWORDS

applications, coatings, optical properties, theory and modeling

1 | INTRODUCTION

In recent decades the use of greenhouses for the growth of a variety of plants and crops has become more wide spread as they offer better weather resilience, pest control and improved yield qualities during off season growth periods. Plastic, often polyethylene, for use as a greenhouse cladding material has become more commonly used, exceeding the use of glass as a greenhouse material. An example of how the use of plastic claddings outweighs glass greenhouses was given in an article by Chang et al.[1] where they ranked countries in terms of their use of greenhouses. The top five ranked countries at the time were China, Spain, South Korea, Japan, and Turkey, which accounted for >90% of the total global greenhouse coverage with ~95% of the materials used for vegetable greenhouses being plastic. A prime example of the use of polyethylene cladding materials for crop growth is in an often cited location in Spain – Almeria, along the coastal region. At this location there is currently more than 250 km^2 of land covered by polyethylene cladding,[2] easily visible in satellite imagery (Figure 1). These cladding materials are translucent materials that offer good light transmission and also a diffusion of the transmitted light providing a more even light distribution over the plants growing under the greenhouse. The materials used must maximize the transmission of photosynthetically active radiation, but thermal build up in the tunnels is problematic both in terms of welfare of the workforce and because crop yields generally reduce as temperature increase.[3]

The translucent cladding materials are often designed to maximize the transmission and distribution of light over the plants, therefore they generally exhibit low

FIGURE 1 Image of coastal section of Almeria showing the area covered by polyethylene cladding (white section) [Google earth images: Main image-Google earth, © 2018 Google, data SIO, NOAA, U.S navy, NGA, GEBCO. Inset image-Google earth, © 2018 Google, data SIO, NOAA, U.S navy, NGA, GEBCO. US Dept of state geographer. Image Landsat/Copernicus] [Color figure can be viewed at wileyonlinelibrary.com]

reflective qualities. However, as is evident in Figure 1, this low level of reflection appears to offer a more reflective area than the surrounding land mass. This alteration in the local reflectivity of the land mass may be sufficient enough to offer a potential benefit to the environment by altering the surface albedo of the local area. Albedo or surface albedo, is a dimensionless unit with a value expressed on a scale of 0 to 1 (or as a percentage) describing the fraction of incident radiation that is reflected from a surface.[4] A value of 0 indicates a non-reflective surface and 1 is for the highest level of reflection in which no absorption occurs. Typically the albedo is used to describe the reflection of shortwave radiation, which encompasses the ultra violet (UV), visible (vis), and near infrared (NIR) wavelengths.[4] Analysis of satellite data over the years has provided an estimate of the average albedo of the Earth's surface to be ~0.3.[5] This value represents averaging over the entire Earth's surface where albedo values can vary widely depending on the local environment. For example in icy regions there is generally a high albedo value in the region of 0.5–0.9,[4] whereas ocean waters albedo values vary between 0.03–0.4 depending on the solar zenith angle,[6] crop land typically ~0.15–0.3 depending on the crop planted,[7] and urban, developed areas tend to have an average albedo level of 0.09–0.27.[8,9]

Albedo values are often used in Earth climate science studies as they play a key role in the surface and atmosphere interaction. The major concern with climate change at a fundamental level relates to the offset to the Earth's energy balance where the Earth experiences higher retention and absorption of incoming solar radiation compared to that going back into space. This energy imbalance will result in an increase in the Earth's average surface temperatures. A large fraction of the radiation causing heating of the environment is longer wavelength radiation in the near infrared (NIR) region. These wavelengths transmitted from the sun can be reflected or absorbed by gases and clouds in the upper atmosphere or those that reach the ground are absorbed and re-radiated back into space. Gases such as methane and carbon dioxide (CO_2) will re-absorb these wavelengths and emit them back in all directions, including toward the Earth's surface, heating the environment. The presence of these gases occurs naturally allowing for heat retention and maintenance of a global mean surface air temperature of ~14°C (Estimated from a period of 1951–1980).[10,11] However, due to anthropogenic activity there has been an increase in the level of greenhouse gases in the atmosphere and hence higher levels of retention of infra-red radiation, increasing the temperatures of the environment.[11,12] Reducing the level of anthropogenic CO_2 emissions can help combat these problems, but with ever increasing demands on resources, this can prove challenging.

A complementary approach that can help reduce temperatures and offset CO_2 emissions may lie in increasing

the surface albedo of local environments. Several articles have been published examining the impact of increasing the reflectivity of roofing, buildings and paving in urban areas.[9,13,14,15,16] These studies were performed using computer simulations to estimate the potential impact by increasing the surface albedo. Akbari et al.[13] suggested that an increase in the surface albedo of 0.25 and 0.15 for roofing and paving respectively could potentially reduce temperatures and offset CO_2 emission by 44 Gt, while a follow up study by and Menon et al.,[9] suggested the value could be higher, up to 57 Gt. However, other studies looking at the surrounding environments showed that while internal temperatures of the environment inside a building maybe reduced, the outside temperatures in the near vicinity could increase in urban areas, therefore placement of higher albedo surfaces need to be selected carefully to direct the sunlight away from pedestrian areas.[15,16]

Studies on the alteration of the albedo within a local environment have not been limited to urban areas alone, but have encompassed areas where more plants are present such as crop growing regions, both with and without greenhouse films present. Studies examining the impact of plants on the local surface albedo offer some interesting insight. Plant leaves themselves have been shown to offer high levels of NIR reflection, hence a high NIR albedo value. The internal structure of the leaves has large micron scale air gaps[17], which are capable of reflecting infra-red radiation.[18,19] An example of the NIR reflective properties of leaves is demonstrated in Figure 2, which shows the reflection data from the top surface of a strawberry leaf exhibiting strong NIR absorptions and reflections.

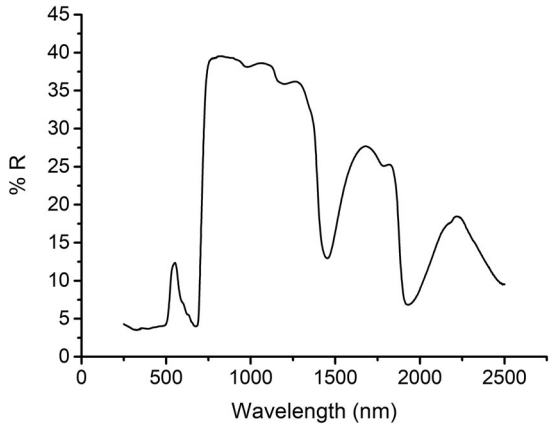

FIGURE 2 Strawberry leaf reflection over the UV–vis–NIR range (250–2500 nm). (data for plot obtained at University of Reading using a Cary 7000 with internal DRA attached. See experimental section for more details)

Doughty et al.[20] simulated how the use of crops with different albedos impacted on the local temperatures of the region. Their observations showed that at low latitudes between ±30° there was less impact on the shortwave radiation reflectivity compared to higher latitudes >30°. Their simulations also suggested that at the lower latitude there may potentially be a negative aspect of impacting on cloud formation and precipitation. They suggested that albedo manipulation of crops may be a desirable option to consider in the higher latitude regions, as the reduction of local temperatures would be more beneficial than crop failure due to the heat; although producing higher albedo crops to cope with possible future warming may prove challenging.

While selective growth of high albedo crops may be an option, it can be limited by how far the albedo of the crop can be manipulated or fairly limiting to what is grown in certain regions. On the other hand the polyethylene films may offset this requirement by offering a sufficient change in surface albedo while any crop desired can be grown underneath it. A study by Campra et al.[21] examined the region in Almeria highly populated by polyethylene greenhouse claddings (Figure 1). They noted a + 0.09 difference in the average annual surface albedo. This average increase had offset the positive radiative forcing (where a positive value means more solar energy is received than radiated back out) attributed to the anthropogenic global increases in greenhouse gases. Fan et al.[22] also made similar observations of an increase in surface albedo due to the use of plastic claddings in areas of China; namely an increase the surface albedo by ~0.17 compared to bare soil under clear cast skies.

The greenhouse cladding materials used are an important design consideration as they influence the photosynthetically active radiation (PAR) directed toward the plants. This, in turn, directly influences the plant growth, quality, and yield achieved.[23,24] PAR radiation occupies a narrow band of the electromagnetic spectrum in the visible wavelength range of 400– 700 nm. Typically the PAR wavelengths are considered the useful wavelengths, although other wavelengths may have an influence on growth, for example Ordidge et al. showed UV radiation improved the development of color and firmness in strawberry plants.[25] At the opposing end of the visible spectrum, NIR radiation can have a detrimental impact on the plants. NIR wavelengths correspond to molecular vibration and rotation energy levels and as a consequence can cause a heating of the environment and potentially a wilting of the plants. The impact on the wavelengths utilized in plant growth must be considered when choosing an appropriate material and the material selected will often be a translucent material, which offers high levels of diffusive light transmission with low levels

of reflection. The diffusivity of light incident on the cladding is a requirement to ensure light is more evenly distributed over the crop under the greenhouse. Polyethylene offers a low cost option for protected crops, while there remain some environmental concerns, it offers considerable strength and with suitable light stabilizers it can last for many years; in addition it is much-lighter than more costly glass options and can be easily moved if circumstances require.[26]

The commercial films we explore here were designed by a team from the University of Reading in conjunction with BPI limited.[27,28]

In this article we examine the optical transmission and reflection data for several commercial materials/films that differ in the light transmission, reflection, and diffusivity, as well as examine a film that offers noticeable impact on the NIR wavelengths. We use UV/visible/NIR spectroscopy to measure the surface albedo of these films and model their properties to help determine how they influence the local environment, such as in the case reported by Campra et al, (2008).[21]

2 | EXPERIMENTAL

2.1 | Materials

Materials/films of polyethylene containing various additives were obtained for analysis. Luminance films, which contain a light scattering additive, were obtained from RPC-BPI. Two sample thicknesses were examined, 150 and 200 μm and a melt blown pure polyethylene film with a thickness of ca. 150 μm was used for comparisons. Two polyethylene films (100 μm and 150 μm) containing a heat reflecting additive were also obtained. The other film was a polyethylene film containing nano-TiO_2.

2.2 | UV–Vis–NIR

UV–Vis–NIR data were obtained on a Cary 7000 Universal Measurement Spectrophotometer equipped with an internal diffuse reflectance accessory (DRA) attachment. This latter attachment was used to obtain Spectra for films normal to the incident light beam over a wavelength range of 200 nm – 2500 nm. A 100% baseline and zero baseline was obtained and all spectra were corrected for these instrument baselines and the scale expressed as a percentage of light transmitted through the film, compared to no film at a given wavelength. This correction is done in the program software following the formula Data = (Scan – zero baseline)/(100% baseline – zero baseline). Both transmission and reflection data were obtained for the films analyzed. The zero baseline measurement was performed by removing the reflectance cap on the DRA and allowing passage of the light beam directly through the integrating sphere section. This results in a low level of reflection being detected from inside the sample compartment, particularly in the NIR wavelength region. Due to the high transparency of the films, the reflection from inside the sample compartment will be detected during reflection measurements, which the zero baseline will compensate for. However this will introduce an over compensation for the transmission data when the reflectance cap is back in place. To compensate for this the original 'Scan' was calculated by rearranging the above formula and the data recalculated using only the 100% baseline, removing the zero baseline over correction.

The universal measurement accessory (UMA) was used to measure the spread of light transmitted/reflected through/from the film. The samples were held at an angle of 0° (sample surface normal to the incident beam) while the UMA detector was rotated from −90° to +90° in 2° detector intervals. 0° here is defined as straight through the sample. A 5° aperture was placed over the detector allowing for ±2.5° coverage of the set detector interval and maximize light collection. A wavelength scan was performed from 200– 2500 nm at each of the detector intervals. Reflection measurements were performed with the sample held at 20°, 45°, and 60°, while the detector was moved to cover angular ranges of −70° to 110°, −45° to 135°, and − 30° to 150° corresponding to the reflections from those sample angles respectively. There is a break in the reflection data between −10° to 10° related to passage of the incident beam. Several samples were run measuring only the specular reflection component of the films by varying samples angle from 10° - 75° in 5° intervals, with the detector set at double the sample angle to measure the specular component (e.g. Sample angle 45°, detector angle 90°). Samples that could not sufficiently support themselves under their own weight were mounted onto a frame with a wide opening and secured in place with tape, to support the film and allow un-interrupted passage of the incident light beam. The wavelength scans were corrected for the instrument baseline and are again expressed as a percentage of light transmission/reflected through/from the sample compared to the transmission with no sample present at a given wavelength. The data files were reduced using a Python script to extract intensity values for given detector angle at particular wavelengths. Area integrations of data plots were carried out using the software package OriginPro 9.1 (OriginLab Corporation, Northampton, MA).

2.3 | Thermogravimetric analysis

Thermogravimetric analysis (TGA) was performed using a TGA-Q50 (TA Instruments) at the Chemical Analysis facility at the University of Reading, UK. Small sections of the films were cut and loaded into an aluminum pan. Samples ranged in masses from 4 to 10 mg and were heated from ~30 to 580°C. The heating rate was 20°C/min under a constant purging gas flow of nitrogen (60 ml/min). Weight loss changes were analyzed using TA Universal Analysis 2000 (Version 4.5A) software package.

2.4 | Scanning electron microscopy

Samples were examined in the FEI Quanta 600 field emission gun scanning electron microscope (FEI, Eindhoven, Netherlands), at the Chemical Analysis Facility, University of Reading, UK. To fracture the films each sample was mounted to a cryo stub secured in a specimen shuttle, which was plunged into nitrogen slush at −210°C. The shuttle was then transferred under vacuum to the Quorum PP2000T cryo-SEM preparation chamber (Quorum Technologies Ltd, UK) at −190°C in which the samples were fractured with a knife. The fractured samples were then removed from the preparation chamber allowing them to warm up to room temperature and each one mounted to an aluminum SEM stub using a double-sided adhesive carbon tab. Remains left in the TGA pans were also taken for analysis. Here a small section of double-sided sticky conducting carbon tab was taken and used to attach any remains in the bottom of the pan to the tab, which was then placed on an aluminum stub. Samples were examined as is, without any coating, at room temperature under low vacuum conditions (0.45 Torr) at accelerating voltages of 12.5–20 kV.

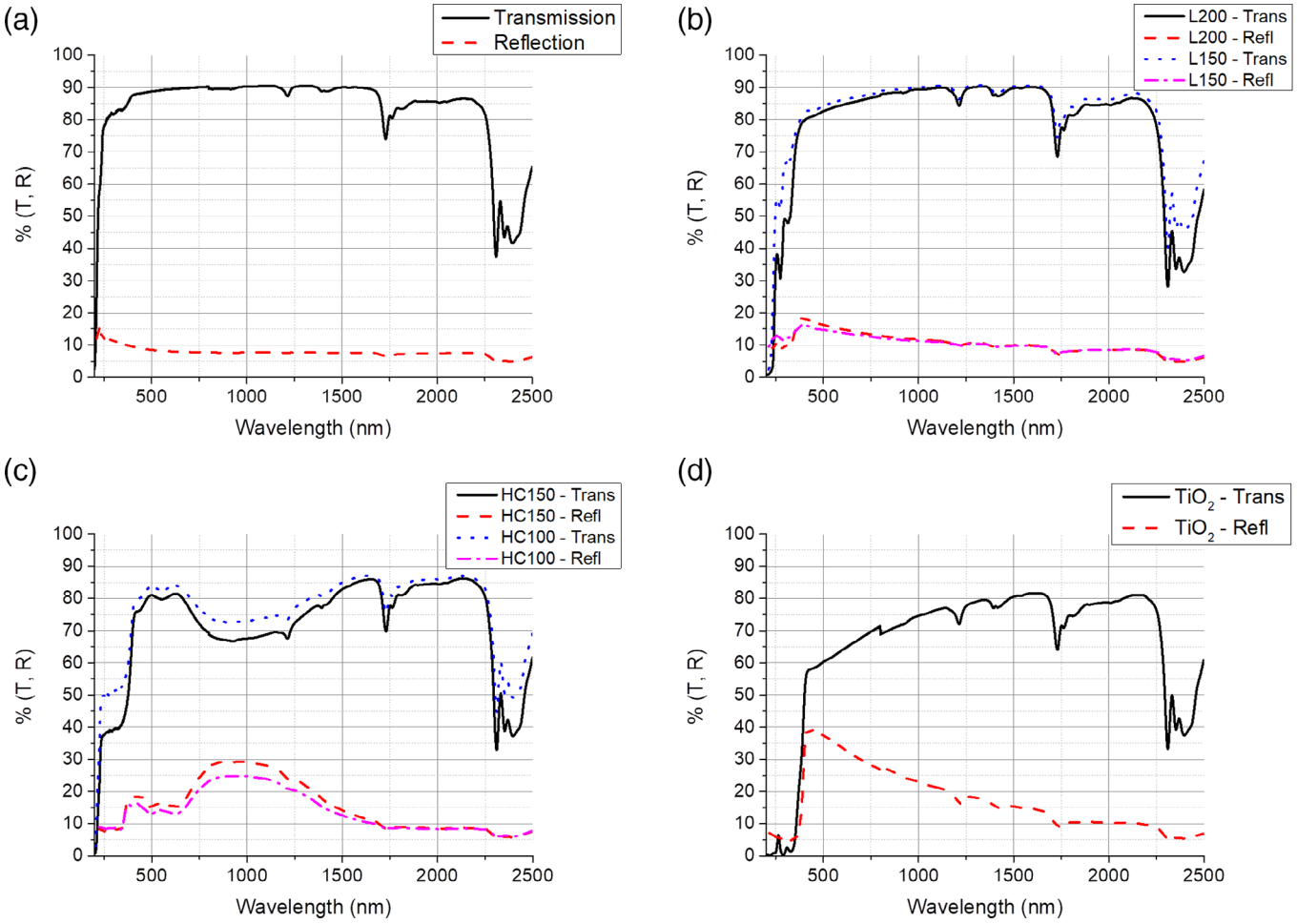

FIGURE 3 Transmission (trans) and reflection (Refl) graphs for (a) pure polyethylene and (b) luminance 150 μm (L150) and 200 μm (L200) thicknesses (c) heat control films 100 μm (HC100) and 150 μm (HC150) thicknesses, and (d) nano-TiO_2 film [Color figure can be viewed at wileyonlinelibrary.com]

3 | RESULTS AND DISCUSSION

Figure 3 below presents the transmission and reflection spectra for the pure polyethylene film (Figure 3(a)) both Luminance films (Figure 3(b)), the heat control films (Figure 3(c)) and the film containing TiO_2 (Figure 3(d)).

We can see from the data in Figure 3 that each film offers quite different transmission/reflection profiles. Examination of the NIR region (700– 2500 nm) reveals a series of peaks common to all films. The largest absorption peak present at ~2300 nm corresponds to the C—H bond and the smaller peaks at ~1700 nm and ~ 1200 nm corresponds to the C—H bonds 1st and 2nd overtones (harmonics) respectively.[29] The transmission levels of the pure polyethylene (Figure 3(a)) and the luminance films (Figure 3(b)) differ by up to ~8% from each other, mainly in the visible part of the spectrum. The Luminance samples possessing a sample thickness of 150 μm maintains an approximately constant overall transmission value (with the exception of the absorption peaks) at ~90% transmission between 800–2500 nm, similar to that of the pure polyethylene film. Moving from the longer wavelength to a lower one (right to left), below 800 nm there is a drop in the transmission with a corresponding increase in the reflection between 800–400 nm, dropping in transmission from ~90% at 800 nm to ~80% at 400 nm. Below 400 nm there is a more rapid fall off in the transmission, which we attribute to a UV absorbing additive explaining why a similar observation is not noted in the pure polyethylene film (Figure 3(a)). The 150 μm film has a 1%–2% higher transmission level compared to the thicker 200 μm sample.

The heat control polyethylene films differ significantly from the pure polyethylene film and the Luminance films. The heat control additive in these films acts as a reflecting material for NIR radiation between 700–1600 nm. This results in a large dip in the transmission profile (Figure 3(c)) and a corresponding large peak in the reflection spectra between these wavelengths for these samples. The additive appears to impact on the visible spectra slightly, lowering its transmission to ~85%, and ~ 80% for the thinner and thicker films respectively. At a wavelength of 700 nm we observe ~10% and 13% lower transmission than pure polyethylene and around 7% and 11% lower than the 150 μm Luminance film at the longer visible wavelengths of 700 nm for the thinner and thicker heat control films respectively. As the transmission decreases with decreasing wavelength for the Luminance films we see their transmission level approach that of the heat control films at around 500 nm. Here there is 5% and 8% difference from pure polyethylene and 1% and 3% for the 150 μm Luminance film when compared to the thinner and thicker heat control film respectively. In addition to the lower transmission levels of the visible light there is also a slight dip around 560 nm in the transmission by ~1% and a corresponding peak present in the reflection spectra. It appears this material has a slight preferential reflection of this particular visible wavelength, at least with the sample surface normal to the incident beam.

Examining the film containing TiO_2 (Figure 3(d)), starting at the longer wavelengths and moving across to the shorter ones (right to left), the TiO_2 film exhibits a more noticeable decrease in the percentage transmission with decreasing wavelength over the entire profile. At 1600 nm there appears to be a steady decline in transmission intensity with decreasing wavelength, changing from ~82% to 70% at 800 nm. Below 800 nm the rate of which the transmission falls off increases. At 700 nm the transmission reaches 68% and by 400 nm has dropped to 58%. Below 400 nm, the UV region, there is a precipitous drop to near 0% transmission. This is probably related to TiO_2 possessing an optical bandgap energy (3.1 eV)[30] below the energy of the UV light, and hence strong photoabsorption in the UV region of the spectra, although this can be modified by manipulating the titania nanostructure.[31] The transmission decreases arise due to the titania doped sample switching character from reflective at the longer wavelengths to absorbing at shorter wavelengths.

Thermogravimetric analysis data was consistent with the spectra shown above. The additives had little effect on the thermal stability of the films, which in all cases were stable up to 300°C, and with the exception of some small (about 10%) weight loss for the luminance 200 μm film, all showed a single decomposition peak with a 50% weight loss at about 474°C for the polyethylene and (481–483)°C for the other 5 samples. Decomposition of the organic material was complete above 500°C leaving (except for the polyethylene) a small amount of residue, which was consistent with the additive. In the case of the luminance films the residue accounted for between 8% and 10% of the sample; for the heat control films between 1% and 2%. For the titanium dioxide containing film the residue accounted for less than 1%; consistent with examples seen for prototype films.[32]

We further looked at the films using SEM; from fractured polymer films the additive could only be observed in situ for the luminance films Figure 4 (a) (presumably the concentration of the other materials is rather low). However, the residues from the TGA experiments allowed us to look at the particle sizes of the additives. Thus the luminance consists of a wide mixture of particle sizes and shapes but typically with dimensions around 1–2 μm (Figure 4(b)) commensurate with predominantly

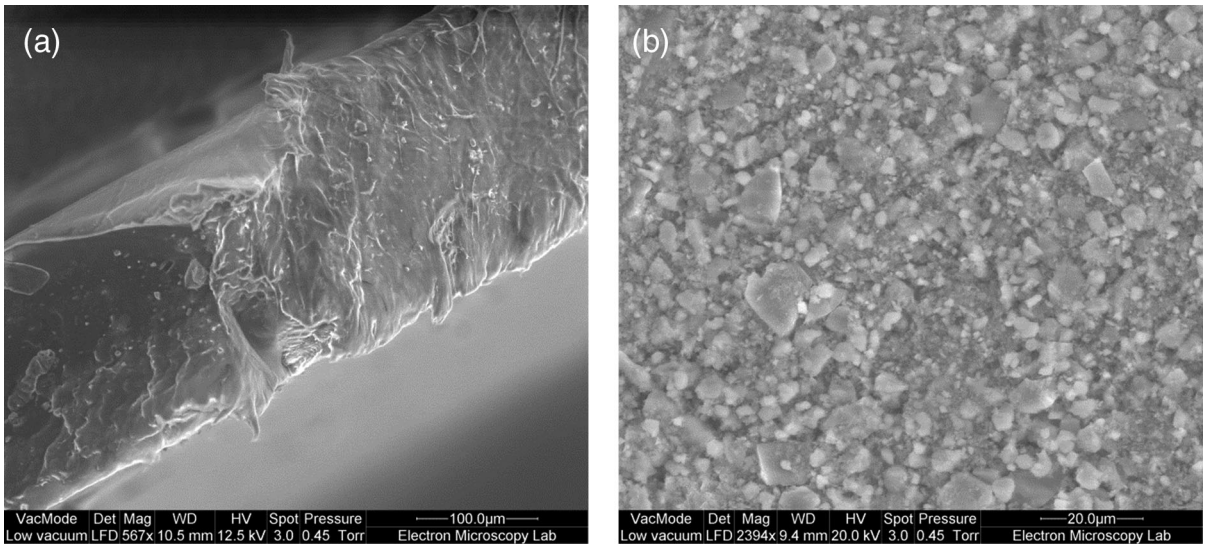

FIGURE 4 SEM micrographs from (a) cross section of the luminance film 200 µm thick (b) residue in the TGA pan from the film

forward Mie scattering behavior.[33] A similar analysis with the TiO_2 films revealed broadly spherical particles with diameters below ca. 400 nm commensurate with, at least some, Rayleigh scattering. The heat control, NIR reflecting films consisted of much larger particles (>10 µm) than would be effective in scattering visible light rather consistent with an inorganic substrate coated with metal oxide.[34] This is typical of many commercial NIR reflecting additives.[35]

The transmission and reflection data are essential to model how much solar energy is absorbed/reflected from the greenhouse cladding materials. Infrared (IR) radiation consists of wavelengths in the range of 700 nm – 1 mm. This form of radiation excites molecular vibrations and rotations, hence heating the environment or material. Approximately 50% of the energy in the form of solar radiation falls in the Infrared range with the majority of this in the NIR range 700–2500 nm. Minimizing the level of NIR entering an environment can help in reducing the environmental temperature, which is particularly necessary for adequate plant growth in warmer climates where wilting can occur. Figure 5 shows the solar irradiation spectra from the sun. The two lines present represent the extra-terrestrial solar irradiation above the atmosphere (Figure 5 - black solid line) and the other (Figure 5 - red dashed line) is a direct beam reference for irradiance reaching the surface through 1.5 air masses (solar zenith ~48°). Here direct beam refers to the direct beam component (plus a contribution from a circumsolar component) from the sun and does not include diffuse sky scatter. Various molecules in the atmosphere such as water molecules result in the absorption of some of the NIR wavelengths, hence the drops to near zero in intensity reaching the Earth's surface at certain wavelengths.

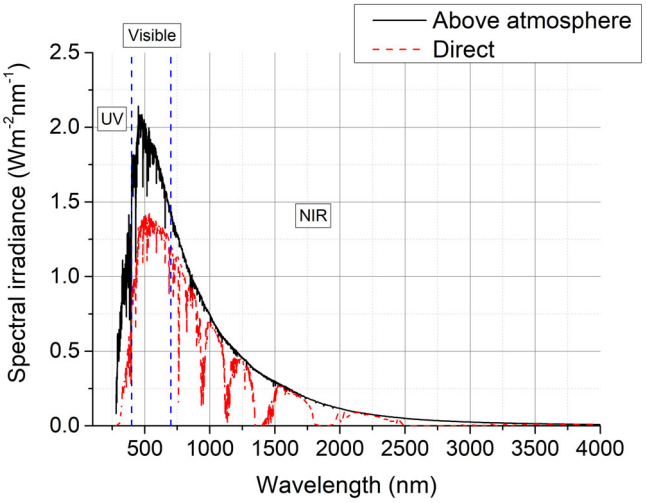

FIGURE 5 Spectral radiation spectrum above Earth's atmosphere (solid line) and for the direct beam component at surface level accounting for travel through 1.5 air masses at a solar zenith of ~48° (dashed line) (ref: National Renewable Energy Laboratory (NREL)-reference air mass 1.5 Spectra[36]) [Color figure can be viewed at wileyonlinelibrary.com]

We can use these data along with the transmission/reflection measurements for the films in Figure 3 to calculate the spectral radiation spectrum at ground level after transmission through the cladding material and also estimate how much radiation is reflected. This can be done simply by multiplying the spectral radiation reaching ground level, $S(\lambda)$ (data for which is obtained from the National Renewable Energy Laboratory [NREL][36]) for a particular wavelength, by the transmission, $\tau(\lambda)$ (or reflection, $R(\lambda)$) data from the film at the same wavelength i.e. $S(\lambda)\tau(\lambda)$ (or $S(\lambda)R(\lambda)$). An example of the calculated spectral irradiance transmitted through

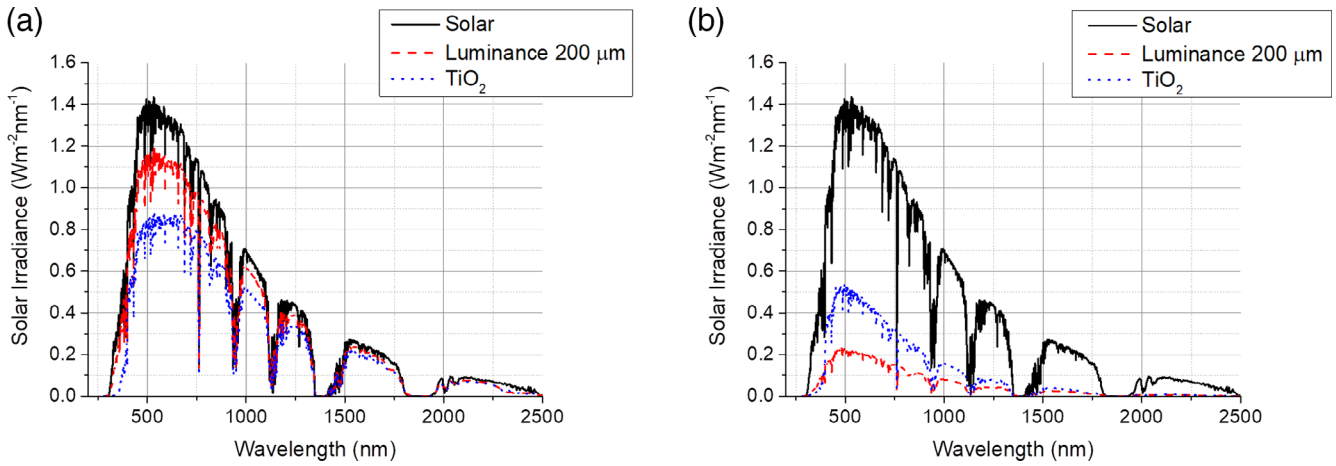

FIGURE 6 Calculated spectral irradiance (a) transmitted through and (b) reflected from the greenhouse cladding materials [Color figure can be viewed at wileyonlinelibrary.com]

TABLE 1 Breakdown of the, UV, visible (Vis), NIR, visible to NIR (VtoN) and total (T) transmission and albedo values calculated for the films and strawberry leaf. (due to fluctuations in sample thickness across the length of the sample, which can influence transmission/reflection data, we estimate an error of ±0.020 on each result)

Sample	UV trans	α_{UV}	Vis trans	α_{vis}	NIR trans	α_{NIR}	VtoN trans	α_{VtoN}	Total trans	α_T
Pure polyethylene	0.848	0.101	0.890	0.084	0.883	0.076	0.886	0.079	0.885	0.080
Luminance 150 μm	0.772	0.151	0.851	0.143	0.879	0.110	0.867	0.124	0.864	0.125
Luminance 200 μm	0.718	0.158	0.835	0.156	0.867	0.114	0.853	0.132	0.848	0.133
Heat control film 100 μm	0.598	0.133	0.825	0.142	0.761	0.199	0.789	0.174	0.783	0.173
Heat control film 150 μm	0.500	0.140	0.795	0.165	0.715	0.232	0.750	0.203	0.742	0.201
TiO_2	0.197	0.113	0.622	0.351	0.731	0.217	0.683	0.275	0.667	0.270
Strawberry leaf	0.001	0.037	0.090	0.063	0.430	0.334	0.282	0.216	0.273	0.210

and reflected from the films is shown below in Figure 6 (a) and (b), respectively for Luminance 200 μm and TiO_2 films.

In a similar fashion, we can calculate the transmission and albedo related to the film in a given spectral waveband by integrating the film impacted solar spectrum data compared to the unimpeded solar spectral data reaching ground level using the following expressions.[27]

$$Trans = \frac{\int S(\lambda)\tau(\lambda)d\lambda}{\int S(\lambda)d\lambda} \quad (1)$$

And

$$\alpha = \frac{\int S(\lambda)R(\lambda)d\lambda}{\int S(\lambda)d\lambda} \quad (2)$$

where *Trans* is the calculated value based on light transmission through the film and α is the albedo related to film reflection, $S(\lambda)\tau(\lambda)$ *and* $S(\lambda)R(\lambda)$ were calculated previously and are described above. The integral limits correspond to the desired waveband of study. In this paper we will calculate several *Trans* and α values, indentified by the subscripts *UV*, *vis*, *NIR*, *VtoN*, and *T*, where the wavebands for the *UV* are 280–400 nm, visible (*vis*) spectra are 400–700 nm, the *NIR* spectra 700–2500 nm, visible to NIR (*VtoN*) as 400–2500 nm and the total (*T*), range is 280–2500 nm. The calculated values from Equation 1 and 2 are given in Table 1. The values lie between 0 and 1 where for *Trans* values 0 is non-transmissive and 1 is the max possible transmission, allowing all light through. For the α values 0 is minimal reflection and 1 is maximum reflection.

The data in Table 1 summarizes the results in Figure 3 averaged over the desired wavelength range

and expressed as a single value. Here we mainly focus on the visible and NIR wavelengths as impacting these offer the biggest contribution to crop development. The pure polyethylene sample again displays the highest levels of transmission of the films studied in this case, with 89% transmission across the visible spectrum of 400 nm – 700 nm. The two Luminance films offer the next highest light transmission values at 85% for the 150 μm film and 84% for the 200 μm thickness film. The decrease in transmission levels can be attributed to the increase in thickness of the sample, resulting in more photon to polymer/additive interactions on route through the film. This will result in an increase in light scattering, broadening the width of the scattered light cone transmitted through the film but also increasing the light back scattered from the film and increasing attenuation, hence the reduction in transmittance levels. A similar situation is observed with the heat control films where the thicker film, again results in a lower overall transmission, dropping by 3% to ~80% transmission in the visible at 150 μm thickness compared to ~83% light transmission for the 100 μm thick sample. These visible light transmissions are 2% and 5% lower than that of the 150 μm Luminance films. However, the heat control films are designed to work in the NIR wavelength region where transmission levels are ~12% lower when comparing the 100 μm heat control film to the 150 μm luminance and 15% lower for the 150 μm heat control film compared to 200 μm thick Luminance film. The film containing nano-TiO_2 is the film with the weakest visible transmission at 62% overall, but also offers only 73% total NIR transmission.

As the albedo data relates to reflection of the incident flux, in the absence of absorption it will broadly increase where the transmission is low. Whereas the pure polyethylene film previously exhibited the better data in terms of light transmission, here it possesses the lowest calculated surface albedo of the films at only ~0.08. Comparing the two thicknesses of the Luminance films we can see that the thicker Luminance film results in a higher α_{vis} compared to the thinner Luminance film, increasing from 0.143 to 0.156, however there is a much smaller difference in the α_{NIR} values of the films ($\Delta\alpha_{NIR} = 0.004$). Interestingly in the data in Table 1 we can see that the α_{vis} values for the Luminance 150 μm film and the 100 μm heat control film are similar at ~0.14. The thicker film with the heat control film at 150 μm has a slightly higher $\alpha_{vis} = 0.165$ compared to the 200 μm Luminance film with $\alpha_{vis} = 0.156$. These values are within 0.01 of each other despite the lower total visible transmissions which maybe a result of the additive causing additional attenuation in the film, hence the lower transmission, despite similar reflections. The real difference in albedo between the Luminance and heat control films is evident when looking at the α_{NIR} values where the heat control films exhibit the larger albedo value ~0.20 and ~ 0.23 for the thinner and thicker samples respectively. This is approximately a + 0.09 and + 0.12 increase in the surface albedo when making a like for like comparison to the thinner and thicker Luminance films respectively. The albedo values represent the reflection of the incident flux away from a surface so an increase in the albedo would be expected with the thicker heat control film having less transmittance, therefore more photon to polymer/additive interaction and greater back scatter. This is evident from the increased albedo value for the thicker heat control film and the increase in reflection of NIR (Figure 3(c)). Finally the film containing the nano-TiO_2 offers the highest level of α_{vis} at 0.35 and second highest α_{NIR} at ~0.22. Although the α_{NIR} is 0.13 lower than the α_{vis} value, it still offers one of the higher albedo's of the films studied in this paper.

We have used the data in Table 1 to calculate the amounts of light reflected back from the structure assuming there is a substantial crop growing by using the reflection data from the strawberry leaf (Figure 2); the results are as shown in Table 2. For these calculations a simple ray model was assumed with an initial light ray from the sun, I_{Sun} (intensity value of 1), is transmitted through the film with transmission T_{Film}, while a percentage of light is reflected from the film surface (R_{Film}). The light that has passed through the film, reflects off a leaf surface with a reflective value of R_{Leaf} and back out the structure, where again the light is reduced by a factor of T_{Film} as it passes through. Each step reducing the intensity of the initial ray based on the transmission and reflection properties of the film and the reflective properties of the leaf. This is a similar approach to that carried out by Fan et al, (2015)[22] who examined the difference in reflection from the ground surface with and without the plastic tunnels present. The above situation we have described accounts for reflection from one leaf leading to

TABLE 2 Visible and NIR total reflection values from films assuming a crop is grown underneath. (values calculated using equation 4. Number of strawberry leaf reflections m = 3)

Sample	Visible light reflected (%)	NIR light reflected (%)
Pure Polyethylene	13.4 ± 2.6	34.3 ± 2.7
Luminance 150 μm	18.9 ± 2.5	37.8 ± 2.7
Luminance 200 μm	20.0 ± 2.4	37.5 ± 2.6
Heat control film 100 μm	18.5 ± 2.4	40.6 ± 2.4
Heat control film 150 μm	20.5 ± 2.4	41.7 ± 2.4
TiO_2	37.6 ± 2.1	40.9 ± 2.4

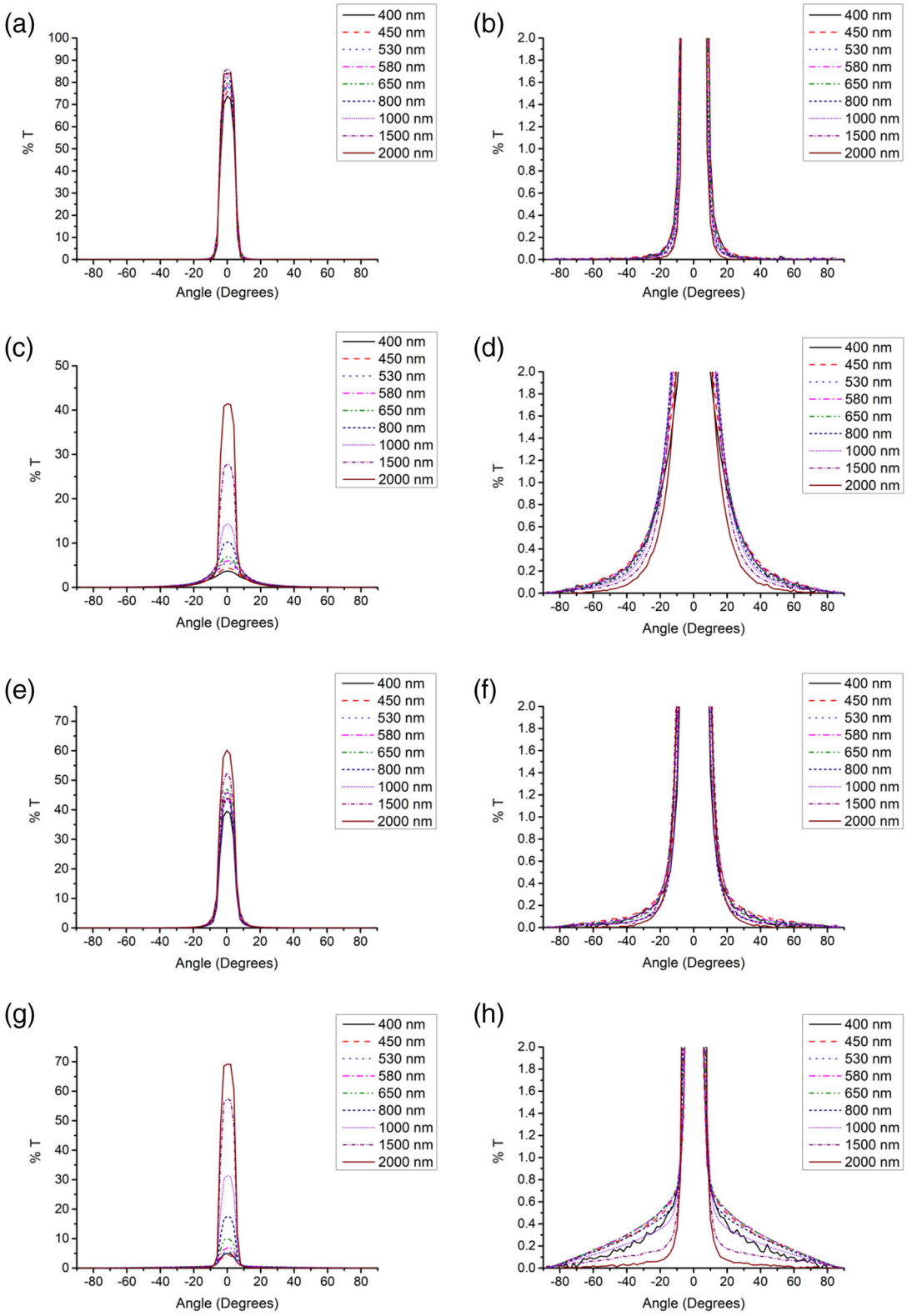

FIGURE 7 Angular distribution of light transmitted through films of (a) and (b) pure polyethylene, (c) and (d) 200 μm luminance, (e) and (f) 150 μm heat control film and (g) and (h) nano-TiO_2 films. Figures (a), (c), (e), and (g) show the entire trasmission profile vs. detector angle while (b), (d), (f), and (h) are the same plot focussing on light intensity transmissions 0<%T<2 [Color figure can be viewed at wileyonlinelibrary.com]

an estimate of the total reflection from the film and one leaf as:

$$R_{Total} = I_{Sun}\left(R_{Film} + T_{Film} \cdot R_{Leaf} \cdot T_{Film}\right) = I_{Sun}\left(R_{Film} + T_{Film}^2 R_{Leaf}\right) \quad (3)$$

If we account for subsequent reflections off the inside of the tunnel and back onto the leaf surface and out again the equation can be modified to account for these additional terms, leading to Equation 4.

$$R_{Total} = I_{Sun}R_{Film} + I_{Sun}T_{Film}^2 \sum_{n=1}^{m} R_{Leaf}^n R_{Film}^{n-1} \quad (4)$$

where R_{Total} is the total reflection out, R_{Leaf} and R_{Film} is the albedo of the leaf and film, respectively and T_{Film} is the transmission of the film. T and R values are based on the values from 0–1 given in Table 1. The summation in Equation 4 accounts for the reflection from the leaf to the film, were it is again reflected back onto another leaf for m total leaf reflections. Additional terms above $n = 1$ tend to offer smaller and smaller contributions to the overall result of R_{Total}.

In line with the spectrum in Figure 2, the leaf contributes very little to reflected light in the visible and consequently the albedo is changed very little; in contrast in the NIR, the foliage substantially increases the light reflected. We can see this reflected in the data in Table 2 where there is a small increase in the visible light reflected, while the NIR has significantly more reflected. The reduction in light will be manifest in a decrease in temperature inside the structures. Of these films the most cooling will be the 150 μm thickness heat control film, followed closely by the titanium dioxide sample, but any advantage of the TiO_2 film is offset by the substantial loss in visible light passing through the film.

Crops will grow better where more of the photosynthetically active radiation is transmitted to them; however, creating an even distribution of light is also a requirement. From the UMA data we examine how the light transmission varies with detector angle. Holding the sample surface normal to the incident beam (Sample angle 0°), we can measure the angular distribution of light transmitted through these films (Figure 7).

We can see from the data presented in Figure 7 that each of the samples have differing amounts of light scatter. The pure polyethylene sample (Figure 7(a), (b)) shows that there is limited scatter of the incoming beam after passing through the film. In contrast the Luminance 200 μm thick sample (Figure 7(c), (d)), the 150 μm heat control film (Figure 7(e), (f)), and the TiO_2 (Figure 7(g), (h)) show improved levels of scatter by comparison to the pure polyethylene film. A common trend among all the samples is the decrease in the broadness of the cone and corresponding increase in central peak transmission through the film with increasing wavelength. Smaller particles have a greater scattering power of the smaller wavelengths. For example, with Rayleigh scattering where the particle size is r<< λ, the scattering intensity, I~1 /λ^4.[37] Thus, nanoscale particles will scatter light quite widely but with low efficiency; with larger particles Mie scattering better describes the situation with forward scattering over small angles predominating; however, the scattering here is more efficient.

We can use the spectrometer data to represent the integrated areas of the light cone to extract information on how much light falls in certain regions. Here we break down the light scattered to regions less than and greater than 30° for a variety of wavelengths ranging from visible to the NIR range. The values extracted from analysis of these light cones can be seen in Table 3 below.

We can see from the data presented in Table 3 that The Luminance and TiO_2 films offer a broader range of scattering compared to the heat control films and polyethylene, which shows practically no scatter beyond 30°. TiO_2 has the strongest scattering; however, this sample also offers a lower overall light transmission. This is most

TABLE 3 Breakdown of the area of the total light scattering cone indicating the amount of light scattered <30° and >30° for a variety of wavelengths

Sample	450 nm		530 nm		650 nm		1000 nm		1500 nm	
	0–30°	30°–90°	0–30°	30°–90°	0–30°	30°–90°	0–30°	30°–90°	0–30°	30°–90°
Polyethylene	99.7	0.3	99.8	0.2	99.9	0.1	99.9	0.1	99.8	0.2
Luminance (150 μm)	89.0	11.0	91.1	8.9	93.2	6.7	96.5	3.5	97.9	2.1
Luminance (200 μm)	87.3	12.7	89.2	10.8	91.5	8.5	95.5	4.5	97.8	2.2
Heat control film (100 μm)	98.8	1.2	99.1	0.9	99.3	0.7	99.5	0.5	99.5	0.5
Heat control film (150 μm)	98.3	1.7	98.8	1.2	99.1	0.9	99.3	0.7	99.4	0.6
TiO_2	78.3	21.8	80.1	19.9	86.3	13.7	95.6	4.4	98.8	1.2

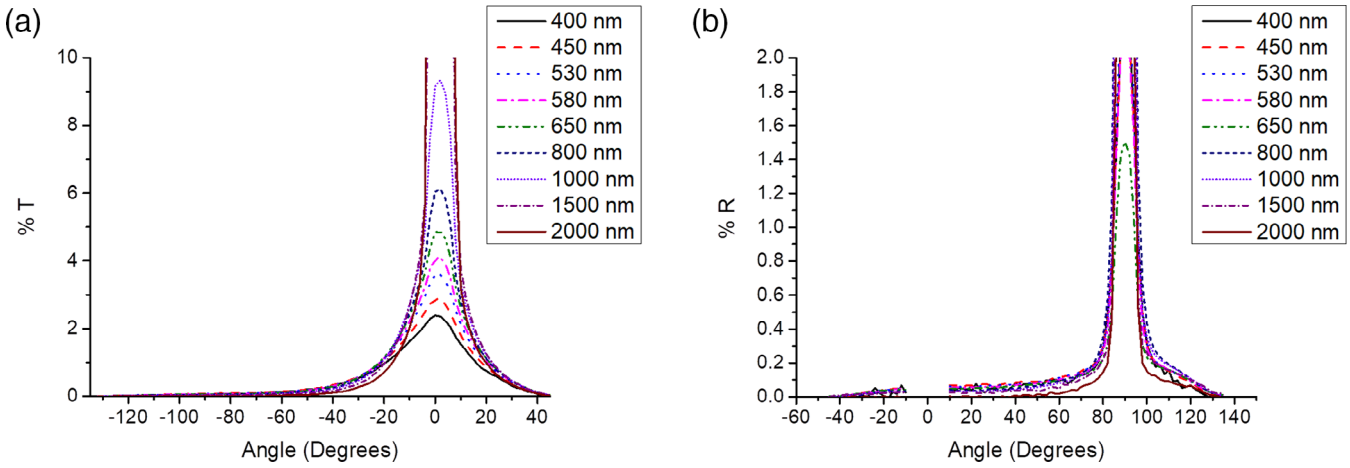

FIGURE 8 Angular distribution of light related to a 200 μm thick luminance film held at 45° with respect to the incident beam, where (a) is the transmission and (b) is the reflection data. (break in reflection data from −10° to +10° due to passage of incident light) [Color figure can be viewed at wileyonlinelibrary.com]

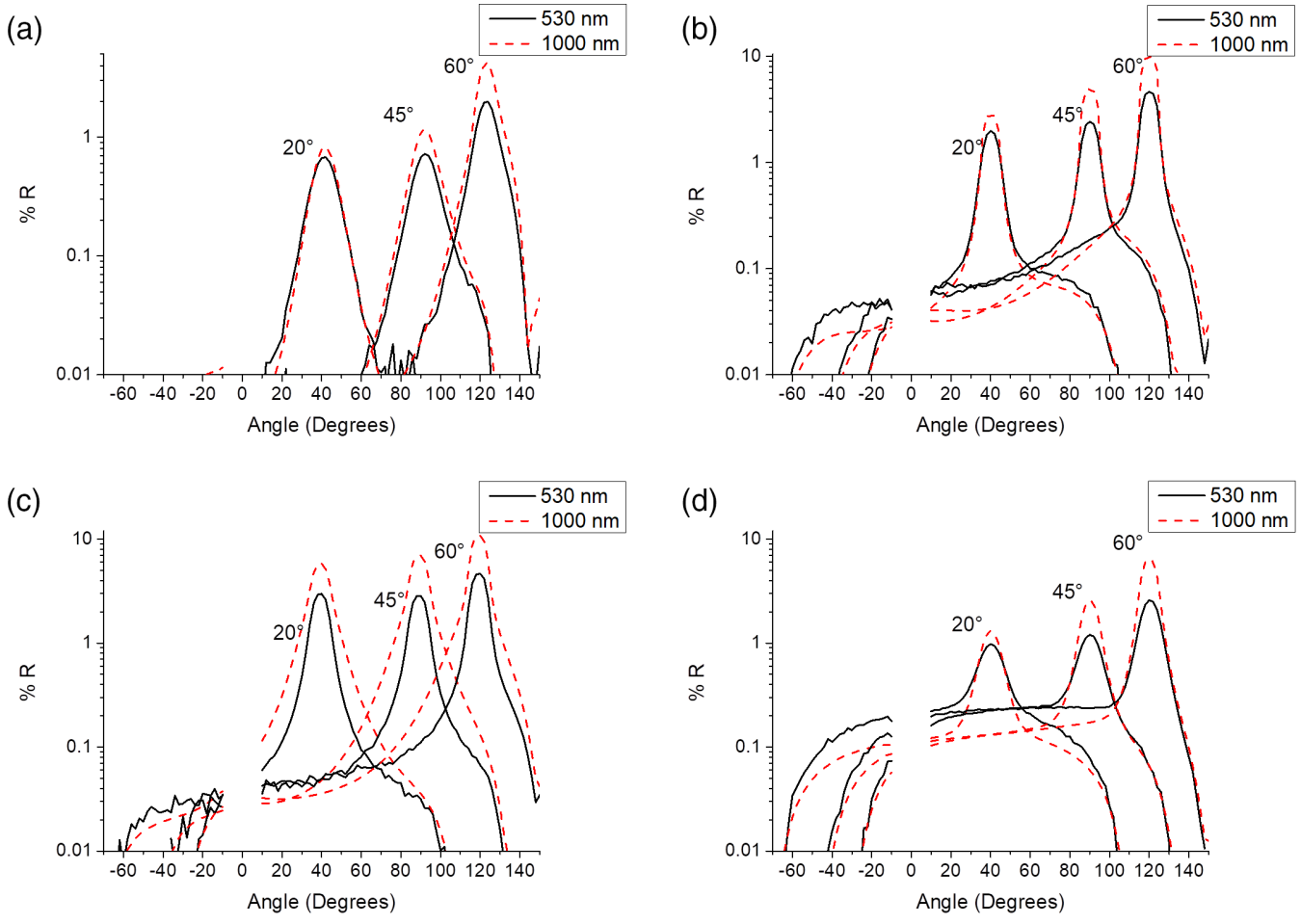

FIGURE 9 Semi-log plots of the 530 nm (black solid line) and 1000 nm (red dashed line) scattering intensity vs. detector angle at angles of incidence corresponding to 20°, 45°, and 60° for (a) polyethylene (b) 200 μm luminance (c) 150 μm heat control film and (d) polyethylene film containing TiO_2. (break in reflection data from −10° to +10° due to passage of incident light) [Color figure can be viewed at wileyonlinelibrary.com]

likely due to light being strongly scattered by the TiO_2 where the scattering power also depends on the refractive index of the material. TiO_2 has a refractive index of 2.65 at 550 nm,[38] much higher than the 1.5 of polyethylene.[39] The scattering of light will occur in all directions, including backwards, hence as the scatter increases the amount of back scatter will also increase which is why we see such a high surface albedo for the TiO_2 film.

The films selected for use will depend on the level of solar irradiance reaching ground at that particular location on the Earth. In general yields increase with greater amounts of photosynthetically active radiation; however, high temperatures may have a detrimental effect on yields; thus, control of the optical properties of films can markedly influence the commercial viability of a crop. Areas of high solar irradiance would allow for the use of the higher reflective films, such as the TiO_2 film, to be used while being able to maintain sufficiently high transmission intensity passing through the film to achieve adequate crop growth. Areas with limited solar intensity would benefit from a film such as Luminance, which maintains a high light transmission while offering good diffusive properties of the light passing through the film.

Thus far we have examined the scattering of light through a sample that is normal to the incident beam, however the greenhouse claddings often have a curved top surface and the sun does not remain at a constant position throughout the day. Using the UMA we can rotate the sample and measure the diffuse transmission and reflection through the sample. An example of this is shown below in Figure 8 for the 200 μm Luminance film at 45° orientation with respect to the incident beam.

Here we can see that the transmission (Figure 8(a)) has some slight asymmetry to the scattering profile. A similar occurrence with the asymmetry in the scattering cone is observed with the reflection data (Figure 8(b)). This asymmetry is present throughout the samples studied in this paper as can be seen in Figure 9, which focuses on the reflection data for two wavelengths, 530 and 1000 nm for four of the samples studied.

The data in Figure 9 is presented in a semi-log plot to emphasize the asymmetry in the reflection cones. We can see that the reflection data in each of the samples exhibits a strong peak that is located at an angle double that of the incident beam angle. This would correspond to a specular reflection component; however, there appears to be a diffusive reflective scatter as well providing intensity at other angles, not solely the specular reflection point. Just as with the transmission data, the most diffusive samples appear to be the polyethylene film containing the TiO_2 additive and the 200 μm Luminance film. A perfect diffusing sample would exhibit a Lambertian scattering profile where the intensity of the scattered light follows a cosine relationship, $I = I_0\cos(\theta)$ where I is the scattered intensity, I_0 is the incident beam intensity and θ is the scattering angle; however, most real objects are not entirely diffusely scattering and exhibit some specular component, as is the case with these films.

The data appears to show that the longer wavelength have higher reflection intensities; however, we attribute this to an overcorrection of the transmission intensity when corrections for the baseline are made in the software. However we can see that much like before with the transmission data, the longer wavelengths are scattered to a lesser degree where the intensity falls off more rapidly with increasing detector angle. There is an exception with the heat control film, which shows a broader reflection cone at the 1000 nm wavelength. The additive in this case is strongly reflective of these wavelengths and appears to be scattering the NIR wavelengths in all directions more strongly than the visible wavelength of 530 nm.

Measuring the specular component of the reflections for above films provides the data shown in Figure 10. We can see here that there is a similar formalism to that following the Fresnel equation for a dielectric material[40,41]:

$$R_{(spec)} = \frac{K}{2}\left[\left(\frac{\cos\theta - \sqrt{n^2 - \sin^2\theta}}{\cos\theta + \sqrt{n^2 - \sin^2\theta}}\right)^2 + \left(\frac{n^2\cos\theta - \sqrt{n^2 - \sin^2\theta}}{n^2\cos\theta + \sqrt{n^2 - \sin^2\theta}}\right)^2\right] \quad (5)$$

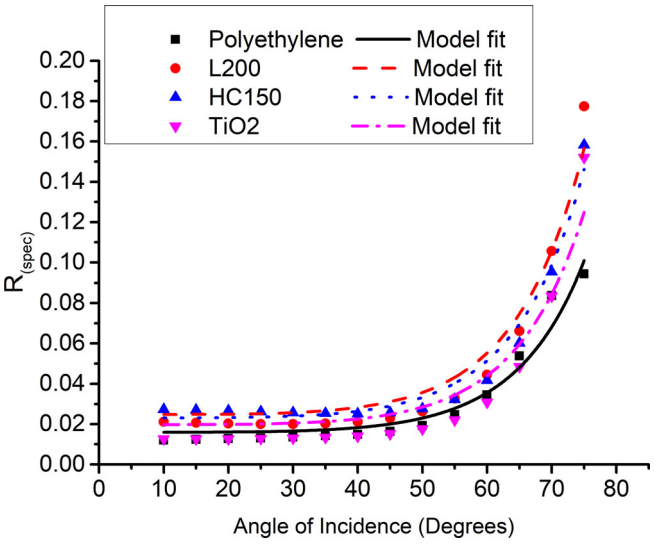

FIGURE 10 Specular reflection measurements of intensity vs. angle of incidence for a 530 nm wavelength. Intensity vs. angle data are provided for the films of polyethylene (■), 200 μm luminance (L200) (●), the 150 μm heat control film (HC150) (▲) and the film containing the TiO_2 additive (▼). The lines represent a plot of the equation 5 model fitted to the data where $n = 1.5$ and K is allowed to vary [Color figure can be viewed at wileyonlinelibrary.com]

where $R_{(spec)}$ is the specular reflectance, K is a scaling constant included in this case used to account for a diminished specular component due to partial diffuse reflectance, $n = n_2/n_1$ where n_1 and n_2 is the refractive index of the air and material, respectively, and θ is the angle of incidence. For the data presented in Figure 10 using the 530 nm wavelength, we have plotted the intensity variation with angle of incidence along with the model lines based on Equation 5 where $n = 1.5$ calculated from $n_2 = 1.5$ and $n_2 = 1.0$ (the refractive index of polyethylene and air, respectively) and K is allowed to vary. Although there are differences which probably arise due to some diffusion of the beam, related to surface roughness and scattering additives, variations in the refractive index of the films, probable partial polarization of the beam due to the instrument optics, and accuracy of the measured intensity, the model fit lines do provide an indication that there is some specular component to the observed reflections.

As we have developed an understanding of the reflective properties of the films, we can relate this to the area in Almeria where there is a large coastal region covered with polyethylene claddings (Figure 1). Using data collected by MERRA2 (Global Modeling and Assimilation Office, 2015) accessed through the NASA Power projects data sets (NASA–Prediction Of Worldwide Energy Resources: The POWER Project) over a period since 1981,[42] we can estimate the average of the solar irradiance throughout the year in this region. Figure 11 shows how the irradiance varies hourly and monthly throughout the day over the year. Figure 11(a), (b) show that for Almeria the peak sunlight irradiance is during the month of July. From the Figure 11(a), (b) we can see that the peak solar irradiance is noon throughout the year as would be expected, this corresponds with the period when the sun is highest (Figure 11(c)).

Examining Figure 11(a) we can see that at the peak solar time of 12:00 am there is a difference of ~400 Wm^{-2}

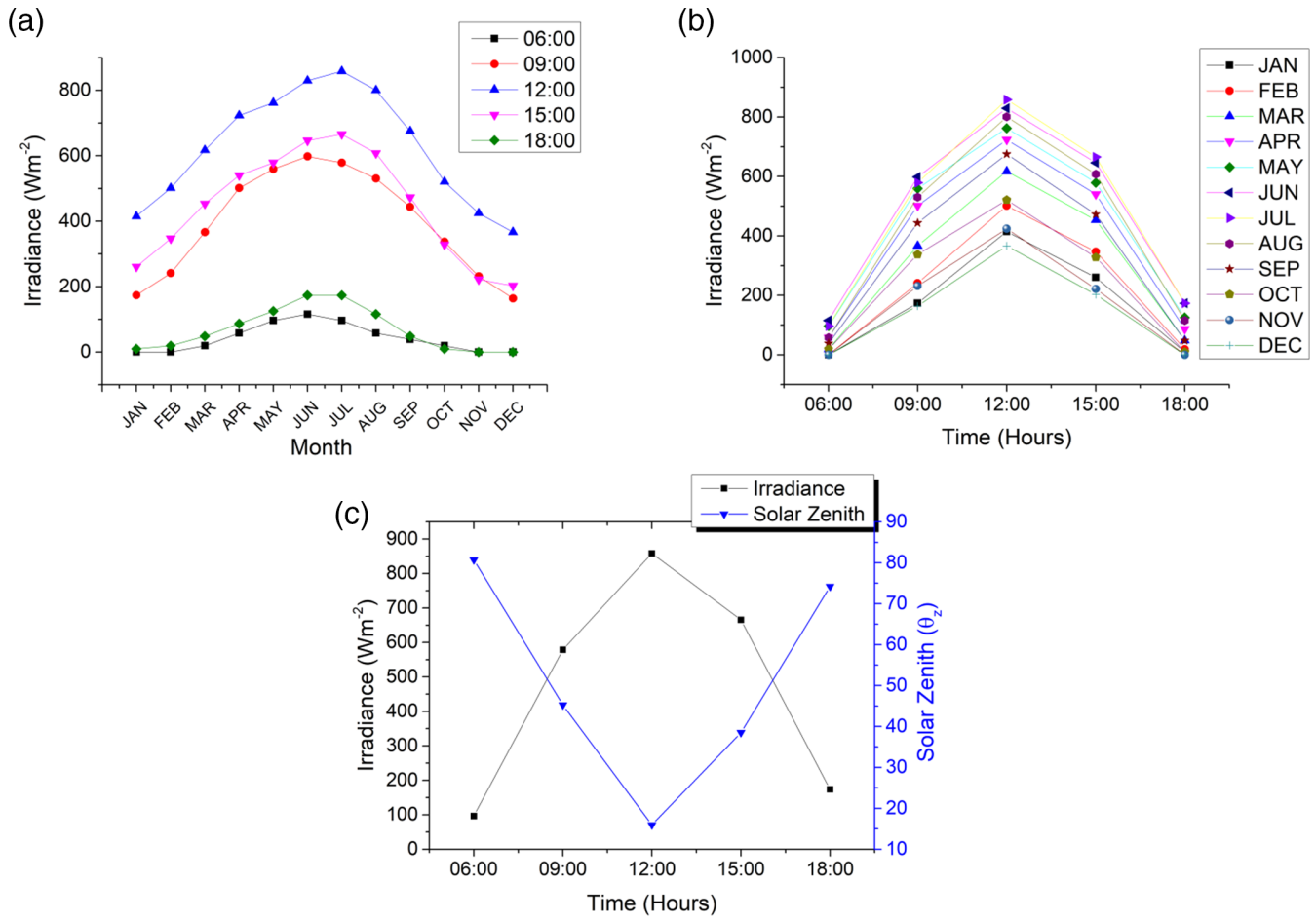

FIGURE 11 (a) Irradiance variation across the year at hours from 6 a.m. to 6 p.m. (b) Irradiance variation across the day showing how it varies from month to month (c) average solar irradiance and solar zenith angle through the day for the month of July [Color figure can be viewed at wileyonlinelibrary.com]

in intensity between the months of January and July. Horticulture in the lower solar irradiance months may very well benefit from a more light transmissive film to account for these lower light intensity months.

Horticultural structures do not always have flat roofs, but can be angled or even curved into a semi-cylindrical type structure. By looking at the data presented above in Figure 9 how the light is reflected from the material at different angles we can develop an understanding of how the light is reflected throughout the day. From Figure 11(c) we can see that at midday the sun is at its highest point in the sky, near directly overhead (Solar zenith angle near 0°). In this situation for a flat roof structure or the top of the curve surface which can be assumed to be flat, it would mimic the situation that we observed for when the sample was held at 0° (normal to the incident beam), and we should see results similar to what was observed in Figure 7, attaining the similar light distribution data (Table 3). If the roof of the cladding is curved, the angle of incidence would be changing across the surface of the film depending on what part of it the light strikes on the surface. The engineered films provide a diffusive reflective scatter in all directions plus a strong specular component. If the sun is overhead, any angle on the surface that corresponds to a surface normal greater than 45° will result in a specular reflection toward the Earth or being directed into the neighboring cladding materials where it will again be scattered. For surface normal angles less than 45° the specular component of the scatter should reflect back out toward the atmosphere. The same principle holds for the sun as it changes its angle overhead throughout the day, although as the sun approaches the horizon the specular reflection angles greater than 45° will be sent upwards to the upper atmosphere rather than being directed down toward the ground. Even though there is a strong intensity specular component, the diffuse scatter in all directions will be providing scatter back into the upper atmosphere of the visible and NIR wavelengths.

Primarily the NIR wavelengths correspond to a heating of the environment, although there is some contribution from the visible wavelengths. The higher albedo materials will reflect more of this energy back toward the upper atmosphere and should therefore provide a greater cooling effect on the local environment than lower albedo materials.

The transmission data show that the most diffusive films will provide a more even distribution of light over the crop throughout the day. Having a limited or no diffusive property in the film may potentially lead to high intensity light in areas causing rapid heating and wilting of the crops or poor distribution prevents light reaching certain plants that maybe shaded by others.

4 | CONCLUSIONS

The use of polymer films is a major factor in food production, offering many advantages in terms of reductions in disease, water use, and protection against climate change. The use of films, such as, those described here is an important factor in making land available for cultivation. However careful design of films is required in order to control of light reaching the plants. This can be achieved through the use of particulates, which scatter light; smaller particulates (diameter<100 nm) scatter in all directions but are not efficient scatterers larger particulates (diameter ca. 1 micron) scatter effectively, but over a narrow range; in all cases higher concentrations increase the scattering, but there is a trade-off between the amount of diffuse light and the total photosynthetic radiation available to the plant. In all these cases reflected light help maintain tunnel temperatures as photosynthesis is inhibited above 35°C, but interestingly have a significant effect on the local climate through additional surface reflections (particularly in the visible region where there is a high solar output). A large component of this is not the reflection from the structure, but through the NIR reflection provided by the crop inside the structure. These data here shows how different treatments can be applied in different circumstances to maximize crop yields.

ACKNOWLEDGMENT

We thank Mr John Phoenix of RPC-BPI for the provision of exemplar films and Innovate UK for funding (Project 102526). We also thank Miss Amanpreet Kaur for her help obtaining the scanning electron microscopy data. Spectral Radiation data were obtained from the NASA Langley Research Center (LaRC) POWER Project funded through the NASA Earth Science/Applied Science Program.

ORCID

Saeed D. Mohan https://orcid.org/0000-0001-5388-088X

REFERENCES

[1] J. Chang, X. Wu, Y. Wang, L. A. Meyerson, B. Gu, Y. Min, H. Xue, C. Peng, Y. Ge, *Front. Ecol. Environ.* **2013**, *11*, 43.
[2] J. A. Aznar-Sánchez, E. Galdeano-Gómez, J. C. Pérez-Mesa, *J. Agrar. Change* **2011**, *11*, 241.
[3] R. R. Shamshiri, J. W. Jones, K. R. Thorp, D. Ahmad, H. Che Man, S. Taheri, *Int. Agrophys.* **2018**, *32*, 287.
[4] A. Roesch, M. Wild, R. Pinker, A. Ohmura, *J. Geophys. Res.* **2002**, *107*, 4221.
[5] J. T. Kiehl, K. E. Trenberth, *Bull. Am. Meteorol. Soc.* **1997**, *78*, 197.

[6] Z. Jin, T. P. Charlock, W. L. Smith Jr., K. Rutledge, *Geophys. Res. Lett.* **2004**, *31*, L22301.
[7] D. Carrer, G. Pique, M. Ferlicoq, X. Ceamanos, E. Ceschia, *Environ. Res. Lett.* **2018**, *13*, 11.
[8] T. R. Oke, *Prog. Phys. Geo.* **1988**, *12*, 471.
[9] S. Menon, H. Akbari, S. Mahanama, I. Sednev, R. Levinson, *Environ. Res. Lett.* **2010**, *5*, 014005.
[10] J. Hansen, R. Ruedy, M. Sato, K. Lo, *Rev. Geophys.* **2010**, *48*, RG4004. https://doi.org/10.1029/2010RG000345.
[11] S. Solomon, D. Qin, M. Manning, Z. Chen, M. Marquis, K. B. Averyt, M. Tignor, H. L. Miller Eds., *IPCC, 2007: Climate Change 2007: The Physical Science Basis. Contribution of Working Group I to the Fourth Assessment Report of the Intergovernmental Panel on Climate Change*, Cambridge University Press, New York, NY **2007**.
[12] T. F. Stocker, D. Qin, G.-K. Plattner, M. Tignor, S. K. Allen, J. Boschung, A. Nauels, Y. Xia, V. Bex, P. M. Midgley Eds., *IPCC, 2013: Climate Change 2013: The Physical Science Basis. Contribution of Working Group I to the Fifth Assessment Report of the Intergovernmental Panel on Climate Change*, Cambridge University Press, New York, NY **2013**.
[13] H. Akbari, S. Menon, A. H. Rosenfeld, *Clim. Change* **2009**, *94*, 275.
[14] H. Akbari, H. D. Matthews, D. Seto, *Environ. Res. Lett.* **2012**, *7*, 024004.
[15] H. Lee, H. Mayer, *Int. J. Biometeorol.* **2018**, *62*, 1199.
[16] M. Taleghani, *Urban Climate* **2018**, *24*, 175.
[17] N. Wuyts, J.-C. Palauqui, G. Conejero, J.-L. Verdeil, C. Granier, C. Massonnet, *Plant Methods* **2010**, *6*, 17. https://doi.org/10.1186/1746-4811-6-17.
[18] S. Jacquemoud, J.-P. Frangi, Y. Govaerts, S. L. Ustin, in *Physical Measurements and Signatures in Remote Sensing* (Eds: G. Guyot, T. Phulpin), A. A Balkema, Rotterdam **1996**, p. 295.
[19] D. C. Castiglione, F. J. Davis, F. J, in *Chapter 10: Copolymer and photonic band gap materials, In: Controlling the Morphology of Polymers: Multiple scales of structure and processing* (Eds: G. R. Mitchell, A. Tojeira), Springer International publishing, AG Switzerland **2016**, p. 263.
[20] C. E. Doughty, C. B. Field, A. M. S. McMillan, *Climatic Change* **2011**, *104*, 379.
[21] P. Campra, M. Garcia, Y. Canton, A. Palacios-Orueta, *J Geophys. Res.* **2008**, *113*, D18109.
[22] X. Fan, H. Chen, X. Xia, Y. Yu, *Atmos. Sci. Let.* **2015**, *16*, 291.
[23] E. Tsormpatsidis, R. G. C. Henbest, F. J. Davis, N. H. Battey, P. Hadley, A. Wagstaffe, *Environ. Exp. Bot.* **2008**, *63*, 232.
[24] C. J. van Haeringen, J. S. West, F. J. Davis, A. Gilbert, P. Hadley, S. Pearson, A. E. Wheldon, R. G. C. Henbest, *J. Photochem. Photobiol* **1998**, *67*, 407.
[25] M. Ordidge, P. García-Macías, N. H. Battey, M. H. Gordon, P. John, J. A. Lovegrove, E. Vysini, A. Wagstaffe, P. Hadley, *J. Sci. Food Agric.* **2012**, *92*, 1597.
[26] G. Scarascia-Mugnozza, C. Sica, G. Russo, *J. Agric. Eng.* **2012**, *42*, 15. https://doi.org/10.4081/jae.2011.3.15.
[27] S. Pearson, A. E. Wheldon, P. Hadley, *J Agric. Eng. Res.* **1995**, *62*, 61.
[28] A. E. Wheldon, F.J. Davis, A. Gilbert, C.J. Van Haeringen, S. Pearson, P. Hadley, J.S. West, R.G. Henbest, Improved Films, European Patent EP1080878A2, **2001**.
[29] D. L. Snavely, J. Dubsky, *J. Polym. Sci., Part A: Polym. Chem.* **1996**, *34*, 2575.
[30] X. Kang, S. Liu, Z. Dai, Y. He, X. Song, Z. Tan, *Catalysts* **2019**, *9*, 191.
[31] C. Dette, M. A. Pérez-Osorio, C. S. Kley, P. Punke, C. E. Patrick, P. Jacobson, F. Giustino, S. J. Jung, K. Kern, *Nano Lett.* **2014**, *14*, 6533.
[32] A. Swinnen, D. Theunynck, A. Delmotte, T. Daponte, Use of Particulate Titanium Dioxide for Reducing the Transmission of Near-Infrared Radiation, WO 2015/052319, World Intellectual Property Organization, **2015**
[33] M. J. Costello, S. Johnsen, K. O. Gilliland, C. D. Freel, W. C. Fowler, *Invest. Ophthalmol. Vis. Sci.* **2007**, *48*, 303.
[34] M. Mennig, P. Oliveira, H. Schmidt, *MRS Proceedings* **1999**, *576*, 415.
[35] H. Jaoua-Bahloul, D. Varieras, E. Beyou, *J. Vinyl Addit. Technol.* **2019**, *25*, E188. https://doi.org/10.1002/vnl.21685.
[36] National Renewable Energy Laboratory (NREL) - Reference Air Mass 1.5 Spectra. https://www.nrel.gov/grid/solar-resource/spectra-am1.5.html. (accessed: July 2019).
[37] B. Santra, M. N. Shneider, R. Car, *Sci. Reports* **2017**, *7*, 40230.
[38] J. R. Devore, *J. Opt. Soc. Am.* **1951**, *41*, 416.
[39] V. E. Henrich, R. L. Kurtz, *Phys. Rev. B* **1981**, *23*, 6280.
[40] R. M. A. Azzam, *J. Opt. Soc. Am. A* **1986**, *3*, 928.
[41] L. G. Coppel, in *Printing on Polymers: Fundamentals and Applications* (Eds: J. Izdebska, S. Thomas), Elsevier, Waltham MA **2016**, p. 307.
[42] NASA – Prediction of Worldwide Energy Resources: The POWER Project. https://power.larc.nasa.gov/ (accessed: July 2019).

How to cite this article: Mohan SD, Davis FJ, Badiee A, et al. Optical and thermal properties of commercial polymer film, modeling the albedo effect. *J Appl Polym Sci*. 2021;e50581. https://doi.org/10.1002/app.50581